Tunable nonlinear refractive index of two-dimensional MoS_2, WS_2, and $MoSe_2$ nanosheet dispersions [Invited]

Gaozhong Wang,[1,2] Saifeng Zhang,[1,4] Xiaoyan Zhang,[1] Long Zhang,[1] Ya Cheng,[3] Daniel Fox,[2] Hongzhou Zhang,[2] Jonathan N. Coleman,[2] Werner J. Blau,[2] and Jun Wang[1,3,5]

[1]*Key Laboratory of Materials for High-Power Laser, Shanghai Institute of Optics and Fine Mechanics, Chinese Academy of Sciences, Shanghai 201800, China*
[2]*School of Physics and the Centre for Research on Adaptive Nanostructures and Nanodevices (CRANN), Trinity College Dublin, Dublin 2, Ireland*
[3]*State Key Laboratory of High Field Laser Physics, Shanghai Institute of Optics and Fine Mechanics, Chinese Academy of Sciences, Shanghai 201800, China*
[4]*e-mail: sfzhang@siom.ac.cn*
[5]*e-mail: jwang@siom.ac.cn*

Received January 6, 2015; revised March 1, 2015; accepted March 1, 2015;
posted March 2, 2015 (Doc. ID 231773); published March 26, 2015

Liquid-phase-exfoliation technology was utilized to prepare layered MoS_2, WS_2, and $MoSe_2$ nanosheets in cyclohexylpyrrolidone. The nonlinear optical response of these nanosheets in dispersions was investigated by observing spatial self-phase modulation (SSPM) using a 488 nm continuous wave laser beam. The diffraction ring patterns of SSPM were found to be distorted along the vertical direction right after the laser traversing the nanosheet dispersions. The nonlinear refractive index of the three transition metal dichalcogenides dispersions n_2 was measured to be $\sim 10^{-7}$ cm^2 W^{-1}, and the third-order nonlinear susceptibility $\chi^{(3)} \sim 10^{-9}$ esu. The relative change of effective nonlinear refractive index $\Delta n_{2e}/n_{2e}$ of the MoS_2, WS_2, and $MoSe_2$ dispersions can be modulated 0.012–0.240, 0.029–0.154, and 0.091–0.304, respectively, by changing the incident intensities. Our experimental results imply novel potential application of two-dimensional transition metal dichalcogenides in nonlinear phase modulation devices.

OCIS codes: (190.0190) Nonlinear optics; (160.4236) Nanomaterials; (160.4330) Nonlinear optical materials.
http://dx.doi.org/10.1364/PRJ.3.000A51

Over the past decade, extensive research on graphene has opened up a door to a new two-dimensional (2D) nanomaterial. Following a similar method to graphene study, scientists have started the investigation of graphene analogues: nanomaterials comprising stacked molecular layers. Layered transition metal dichalcogenides (TMDs) are a major 2D nanomaterial. The chemical composition of TMDs can be expressed in the form of MX_2 (M = Mo, W, Ta, Ti, Nb, etc.; X = S, Se, Te) [1], in which the M layer is sandwiched by two X layers [2].

In contrast to graphene, layered TMDs show some unique photonic and optoelectronic properties. Noticeable improvement in photoluminescence was observed with the transition from indirect band gaps in bulk MoS_2 [3], WS_2 [4], and $MoSe_2$ [5] limits to direct band gaps in their monolayer limits. MoS_2, WS_2, and $MoSe_2$ nanosheets have revealed extraordinary absorption in the visible region, pointing to a method to exploit ultrathin photovoltaic devices [6]. Highly efficient second-harmonic generation was obtained from the bilayer MoS_2 [7]. Recently, we showed that the layered MoX_2 nanomaterials possess excellent saturable absorption for ultrafast pulses in the near-infrared region [8]. In addition, we measured the nonlinear refractive index of the MoX_2 dispersions $n_2 \sim 10^{-7}$ cm^2 W^{-1} and the third-order nonlinear susceptibility $\chi^{(3)} \sim 10^{-9}$ esu. In order to determine $\chi^{(3)}$ for the monolayer of TMDs, in this work, we studied the spatial self-phase modulation (SSPM) of the TMDs dispersions, and found that the nonlinear refractive index can be tuned by controlling the distortion of SSPM patterns. SSPM is a well-known nonlinear optical (NLO) behavior induced by the change of refractive index, which has been observed from the graphene and carbon nanotube dispersions [9,10].

Layered MoS_2, WS_2, and $MoSe_2$ nanosheets were prepared by liquid-phase exfoliation in cyclohexylpyrrolidone (CHP). Experimental and theoretical results show that the surface energy of CHP is sufficient to pay for the energy cost for overcoming the van der Waals between two molecular layers in bulk MoS_2, WS_2, and $MoSe_2$ [1]. The major strategy for preparing the three kinds of dispersions is akin to our previous work on MoS_2 nanosheets [8]. The TMDs dispersions were prepared at an initial concentration of 5.0 mg/mL in CHP. The initial dispersions were then sonicated by a high-power ultrasonic tip for 60 min to exfoliate the bulk TMDs into single or few layers. After sonication, the dispersions were allowed to settle for 24 h at room temperature. The top half of the dispersions were collected, which were then centrifuged at 1500 r/min for 120 min, aiming at removing any large aggregates in the dispersions. The stability and no further sedimentation of the dispersions signified the high quality of 2D TMDs nanosheets in CHP.

The status of the three dispersed TMDs was observed by scanning transmission electron microscopy (STEM). As shown in Figs. 1(a)–1(c), the STEM images imply that the three TMDs can be effectively exfoliated to 2D TMDs nanosheets with the size of a few micrometers. Plenty of well-exfoliated TMDs nanosheets can be seen. Raman

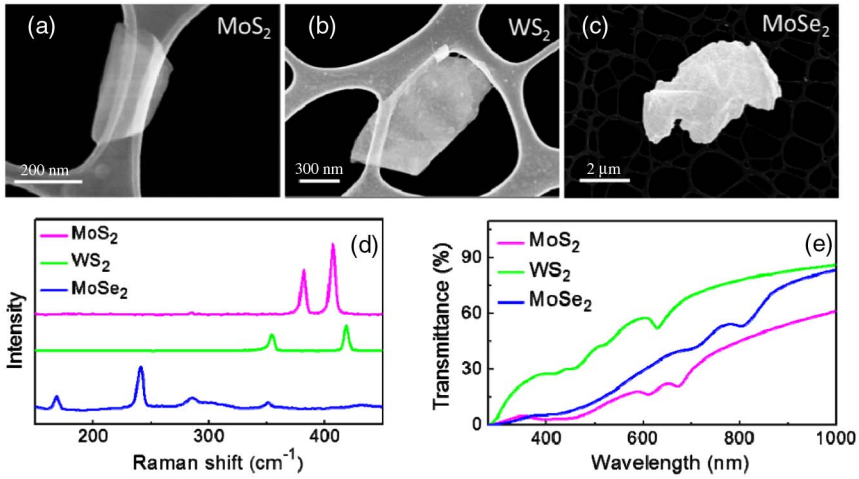

Fig. 1. STEM images of (a) MoS_2, (b) WS_2, and (c) $MoSe_2$ nanosheets. (d) Raman spectra of the three TMDs. (e) Transmittance spectra from 300 to 1000 nm.

spectrum is proved to be a powerful tool for identifying the number of layers of the 2D nanomaterials [5,11–15]. The Raman samples were lying on Si wafer after diluting the initial dispersions. We studied the atomic structure arrangement of the three TMDs using a Jobin Yvon LabRam 1B Raman spectrometer with a laser at 488 nm. Figure 1(d) shows the Raman spectra of MoS_2, WS_2, and $MoSe_2$ nanosheets in the region of 150–450 cm^{-1}. Two characteristic peaks at 382.3 and 406.6 cm^{-1} of MoS_2 are defined as the in-plane E^1_{2g} and out-plane A_{1g} Raman vibrational modes. A mean frequency difference of ~24.3 cm^{-1} between the two modes implies a thickness of less than ~10 monolayers [8,14]. For WS_2, the two phonon modes E^1_{2g} and A_{1g} appear at 355.1 and 418.09 cm^{-1}, respectively. This indicates that the layer number of WS_2 nanoflakes in our experiment is less than ~5 monolayers [15,16]. In the case of $MoSe_2$, the out-plane vibrational mode A_{1g} at 241.0 cm^{-1} showed that the thickness was equivalent to ~3–4 monolayers [5].

In the SSPM experiment, a cw laser beam from an Ar–ion laser (Melles Griot Laser, 35-LAP-431-220) at 488 nm was focused by a lens of focal length 100 mm. The nanosheet dispersions were contained in quartz cuvettes with a pathlength of 10 mm. The front surface of the quartz cuvette was placed on the focus of the laser beam. The diameter of $1/e^2$ intensity at the lens was 0.65 mm. When passed through the dispersions, the laser beam was diverged into a series of coaxial

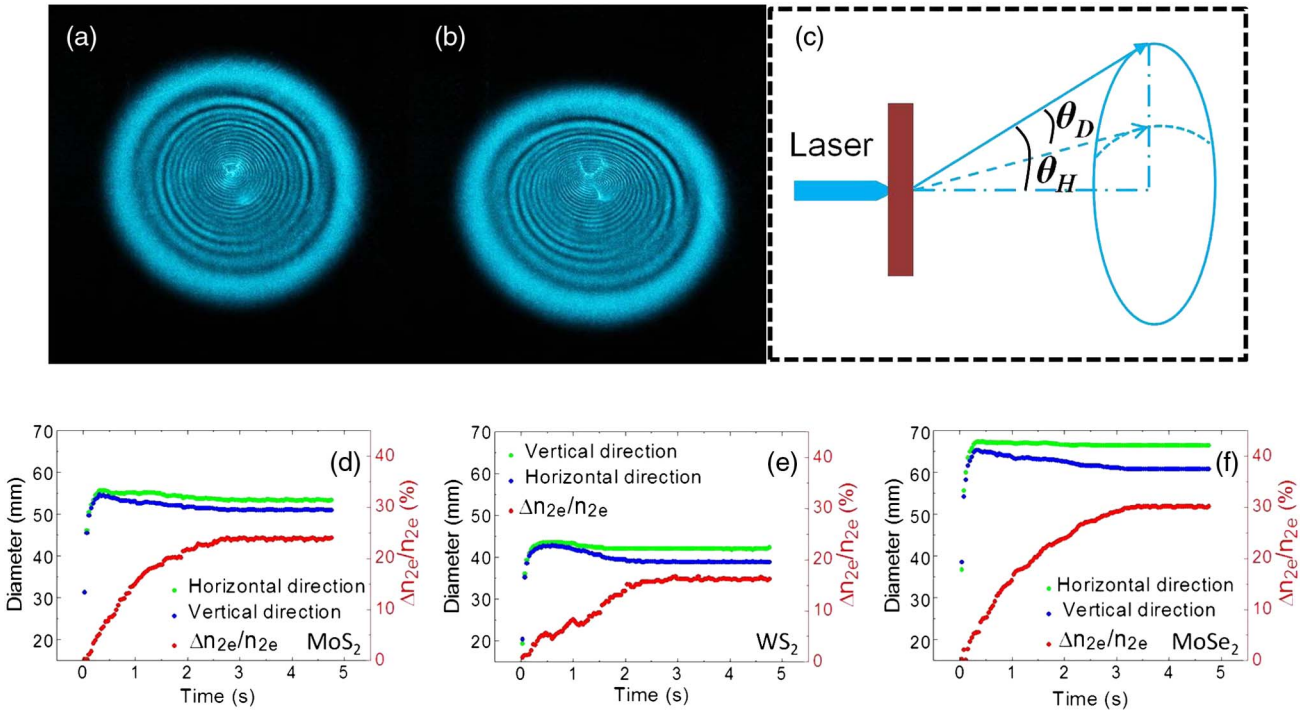

Fig. 2. (a) Typical SSPM diffraction ring pattern and (b) its stable distorted pattern. (c) Schematic of half-cone angle θ_H and distorted angle θ_D. (d)–(f) Diameters of the outermost diffraction ring along the vertical and horizontal directions and $\Delta n_{2e}/n_{2e}$ as functions of time.

diffraction cones. A black screen was put 650 mm away from the dispersions. As shown in Fig. 2(a), due to SSPM happening in the dispersions, a series of concentric diffraction rings shows up on the screen right after the laser traverses the dispersions along the horizontal direction. The nonlinear refractive index and the third-order NLO susceptibility of the TMDs nanosheets can be deduced by analyzing the diffraction rings' patterns. An interesting phenomenon is the distortion of the SSPM diffraction rings' patterns. It can be seen that the initial SSPM diffraction rings' patterns were a series of concentric circles just after the laser passed through the dispersions. However, the upper half of the SSPM diffraction rings was distorted toward the center of the rings in a few seconds, while the lower half stayed the same as shown in Fig. 2(b).

The mechanism of SSPM in the TMDs dispersions is the same as the situation in nematic liquid crystal films and graphene [9,17,18]. According to the optical Kerr effect, the effective refractive index of the TMDs dispersions can be described by [17]

$$n_e = n_{0e} + I n_{2e}, \tag{1}$$

where n_{0e} and n_{2e} are the effective linear and nonlinear refractive indices, respectively, and I stands for the incident laser intensity. An intensity-dependent refractive index change induced by a highly intense laser field gives rise to self-phase modulation. Similar to the case of liquid crystals and graphene [9,17], the change of n_e of the TMDs dispersions is due to the reorientation and alignment of the layered nanosheets influenced by the laser field. When the TMDs nanosheets are irradiated by the laser beam, an electron (hole) is excited to the conduction (valence) band from the valence (conduction) band. The generated electrons and holes will move in opposite directions, being antiparallel and parallel to the electric field, respectively. This would result in polarized TMDs nanosheets. The initial angle between the polarization direction and the electric field will be minimized when the reorientation occurs, resulting in the minimum interaction energy [9,19]. This leads to a local refractive index change n_e of the TMDs dispersions in the optical path and a relevant phase shift $\Delta\psi$ of the laser beam [17],

$$\Delta\psi(r) = \frac{2\pi n_{0e}}{\lambda}\int_{-L_e/2}^{L_e/2} \Delta n_e(r,z)\mathrm{d}z, \tag{2}$$

where r is the radial coordinate of the laser beam, and λ is the vacuum wavelength of the laser. $L_e = \int_{L_1}^{L_2}(1+z^2/z_0^2)^{-1}\mathrm{d}z$ is the effective pathlength contributing to SSPM, where L_2 and L_1 are the on-axis coordinates of the dispersions, $z_0 = \pi w_0^2/\lambda$ (w_0 is the $1/e^2$ beam radius) is the diffraction length at $z = 0$, and $L = L_2 - L_1$ is the thickness of the quartz cuvette. In the experiment, $L = 10$ mm, $w_0 = 33.79$ μm, and L_e is calculated to be 6.89 mm. According to Eqs. (1) and (2), when the refractive index is changed by the incident intensity, the phase shift can be expressed as

$$\Delta\psi(r) = \frac{2\pi n_{0e}}{\lambda}\int_{-L_e/2}^{L_e/2} \Delta n_{2e} I(r,z)\mathrm{d}z, \tag{3}$$

where $I(r,z)$ is the intensity distribution of the focused laser field. The electromagnetic fields on two different r points can interfere when they have the same wave vector, resulting in a series of concentric diffraction rings [Fig. 2(a)] [17]. Estimated

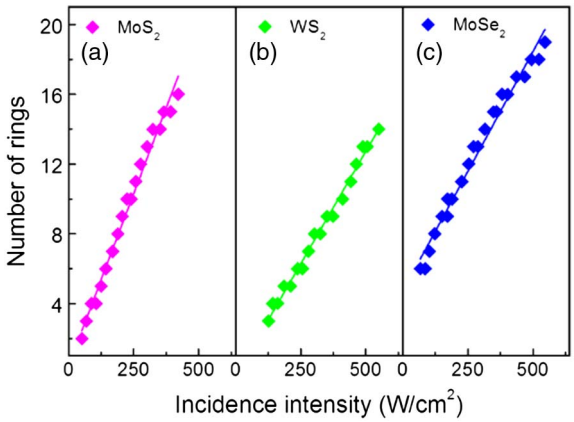

Fig. 3. Numbers of diffraction rings as a function of incident intensity.

from the relation $\psi(0) - \Delta\psi(+\infty) = 2N\pi$, the total number of diffraction rings can be expressed as $N = \Delta\psi_0/2\pi$ [17]. Therefore, the effective nonlinear refractive index can be expressed as [9]

$$n_{2e} = \frac{\lambda}{2n_{0e}L_e}\cdot\frac{N}{I}. \tag{4}$$

As shown in Fig. 3, N is closely proportional to I for all three TMDs, and N/I can then be obtained readily. For the TMDs dispersions, the linear refractive index n_{0e} is close to that of CHP, i.e., $n_{\mathrm{CHP}} = 1.499$. Therefore, the effective nonlinear indices n_{2e} for the MoS_2, WS_2, and $MoSe_2$ nanosheets can be deduced from Eq. (4). The results are given in Table 1.

Third-order NLO susceptibility $\chi^{(3)}$ is an important parameter to measure the nonlinearity of materials. Since $\chi^{(3)}$ of the layered nanosheets can be estimated as $\chi^{(3)}_{\mathrm{total}} = N^2_{\mathrm{eff}}\chi^{(3)}_{\mathrm{monolayer}}$ [9], where N_{eff} is the effective number of the monolayer, and $n_{2e}(\mathrm{cm}^2/\mathrm{W}) = 0.0395\chi^{(3)}_{\mathrm{total}}\,(\mathrm{esu})/n^2_{0e}$, one can obtain $\chi^{(3)}$ for a TMDs monolayer,

$$\chi^{(3)}_{\mathrm{monolayer}}\,(\mathrm{esu}) = \frac{n^2_{0e}n_{2e}(\mathrm{cm}^2/\mathrm{W})}{0.0395\times N^2_{\mathrm{eff}}}. \tag{5}$$

According to Eqs. (4) and (5), N_{eff} is the parameter that needs to be determined in order to estimate $\chi^{(3)}_{\mathrm{monolayer}}$. Following the case of graphene [18], N_{eff} of the TMDs nanosheets can be estimated by $T^{N_{\mathrm{eff}}}_{\mathrm{monolayer}} = T_{\mathrm{total}}$, where T_{total} is the transmittance of the three TMDs dispersions and $T_{\mathrm{monolayer}}$ is the transmittance of a TMDs monolayer. $T_{\mathrm{monolayer}}$ for the MoS_2, WS_2, and $MoSe_2$ monolayers was determined to be 99.4%, 99.70%, and 99.10%, respectively [6]. Since T_{total} of the MoS_2, WS_2, and $MoSe_2$ dispersions in our experiment was 44.79%, 78.26%, and

Table 1. Effective Nonlinear Refractive Indices and Third-Order Optical Susceptibilities of MoS_2, WS_2, and $MoSe_2$

	MoS_2	WS_2	$MoSe_2$
n_{2e} (cm^2/W)	$(9.32 \pm 0.30)\times 10^{-7}$	$(6.09 \pm 0.14)\times 10^{-7}$	$(6.49 \pm 0.14)\times 10^{-7}$
$\chi^{(3)}$ (esu)	$(3.00 \pm 0.10)\times 10^{-9}$	$(5.15 \pm 0.12)\times 10^{-9}$	$(7.75 \pm 0.24)\times 10^{-9}$

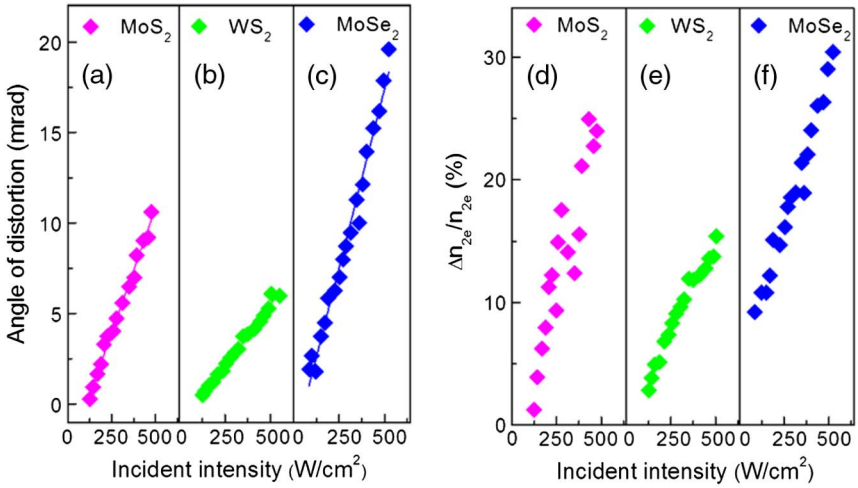

Fig. 4. Distortion angle of (a) MoS_2, (b) WS_2, and (c) $MoSe_2$ as functions of incident intensity. $\Delta n_{2e}/n_{2e}$ of (d) MoS_2, (e) WS_2, and (f) $MoSe_2$ as functions of incident intensity.

53.54%, respectively, the corresponding N_{eff} was estimated to be ~133, ~82, and ~69 for the three dispersions, respectively. As a result, $\chi^{(3)}_{\text{monolayer}}$ of the three TMDs can be obtained by applying N_{eff} and n_{2e} in Eq. (5). The results are given in Table 1.

Due to the SPM effect, a series of concentric diffraction rings was observed after the focused laser beam horizontally passed through the TMDs dispersions, as shown in Fig. 2(a). However, the upper half of the diffraction rings collapsed to the center of the patterns in a few seconds while the lower half remained the same [see Fig. 2(b)]. As shown in Figs. 2(d)–2(f), the diameters of the diffraction rings in the vertical direction reduced dramatically after it increased to a maximum, while those in the horizontal direction decreased slightly after the maximum. Both the diameters reached stable values after a few seconds. This SSPM distortion has been reported in liquid crystals [17], carbon nanotubes [10], dye solutions [20], and graphene dispersions [9,18]. In general, the mechanism of the distortion is attributed to a laser-induced thermal effect. Based on our research in graphene dispersions [18], the SSPM distortion is mainly due to the nonaxis-symmetrical thermal convections induced by the laser beam. The convection induced by laser heating is similar to the onset of convection around a suddenly heated horizontal wire, which was investigated in detail by Vest and Lawson [21]. The three TMDs dispersions will be heated immediately due to their high optical absorption coefficients and thermal conductivities [8,22–24]. This leads to a rising temperature gradient along the vertical direction in the dispersions with a consequence of strong thermal convections around the focus of the laser beam. Therefore, the densities of the TMDs nanosheets, i.e., the effective number of monolayer N_{eff}, decrease in the upper part of the laser beam. According to $n_{2e} = (1.2 \times 10^4 \times \pi^2/n_0^2 c)\chi^{(3)}_{\text{total}}$ and $\chi^{(3)}_{\text{total}} \approx N^2_{\text{eff}}\,\chi^{(3)}_{\text{monolayer}}$, the effective nonlinear refractive index n_{2e} of the TMDs dispersions is linearly proportional to the effective number of monolayer N_{eff}. As a consequence, the upper half of the laser beam is diffracted by the dispersions with the reduced n_{2e}, resulting in the upper part of the diffraction rings distorting toward the center of the patterns, as shown in Fig. 2(b). This is in agreement with the calculation of the half-cone angle of the diffraction. As illustrated in Fig. 2(c), θ_H is defined as the half-cone angle, and θ_D is defined as the distortion angle to study the degree of distortion. θ_H in terms of a Gaussian laser beam can be expressed as [18]

$$\theta_H \approx n_{2e}\left[-\frac{8IrL}{w_0^2}\exp\left(-\frac{2r^2}{w_0^2}\right)\right]_{\max}, \qquad r \in [0, +\infty), \tag{6}$$

where $[-\frac{8IrL}{w_0^2}\exp(-\frac{2r^2}{w_0^2})]_{\max}$ is a constant when $r \in [0, +\infty)$. As a result, θ_H is proportional to the effective nonlinear refractive index of the dispersions. That is to say, n_{2e} can then be tuned by the change of the TMDs concentration caused by the thermal convection, which can be controlled by changing the incident intensity of the laser. As shown in Figs. 4(a)–4(c), all the distortion angles of the diffraction ring patterns of the three TMDs dispersions linearly increase with the increase of the incident intensity.

According to Eq. (6), Δn_{2e}, the change of n_{2e} before and after the distortion, can be deduced in the form of

$$\Delta n_{2e}/n_{2e} = \theta_D/\theta_H, \tag{7}$$

where θ_D and θ_H can be measured readily at different intensities in the experiment. As shown in Figs. 2(d)–2(f), the variation of the diameters of the outermost diffraction rings in the two orthogonal directions indicates the change of the distortion angles, which directly reflect the dynamic change of n_{2e} with time. All $\Delta n_{2e}/n_{2e}$ of the three TMDs dispersions increase fast when the laser passes through them, and stay at stable values after reaching the maximum. From Figs. 4(d)–4(f), we can tell that $\Delta n_{2e}/n_{2e}$ changes linearly with the incident intensities. $\Delta n_{2e}/n_{2e}$ of MoS_2, WS_2, and $MoSe_2$ increase from 1.2%, 2.9%, and 9.1% to 24.0%, 15.4%, and 30.4% when the incident intensity is tuned from 121, 129, and 82 to 487, 503, and 524 W/cm^2, respectively. According to Table 1 and Eq. (7), Δn_e of the three TMDs is tuned up to 0.02, 0.03, and 0.09, respectively, within the above incident intensity range when N_{eff} is set to 2000, larger than electric-field-induced one (~0.01) in some organic materials, say, ATOP dyes [25] and the carrier-induced one (~0.01) in InP, GaAs, and InGaAsP [26].

In conclusion, we present SSPM and its distortion of layered MoS_2, WS_2, and $MoSe_2$ nanosheets prepared by using liquid-phase-exfoliation technology. The nonlinear refractive index of the three TMDs dispersions n_2 was measured to be $\sim 10^{-7}$ cm^2 W^{-1}, and the third-order nonlinear susceptibility $\chi^{(3)} \sim 10^{-9}$ esu. The relative change of the effective nonlinear refractive index $\Delta n_{2e}/n_{2e}$ of the three TMDs dispersions can be spanned from 0.012, 0.029, and 0.091 to 0.240, 0.154, and 0.304, respectively, by changing the incident intensities. These results imply novel potential application of 2D TMDs in nonlinear phase modulation devices.

ACKNOWLEDGMENTS

This work is supported in part by the National Natural Science Foundation of China (No. 61178007, No. 61308034, and No. 51302285), the Science and Technology Commission of Shanghai Municipality (No. 12ZR1451800), the Excellent Academic Leader of Shanghai (No. 10XD1404600), and the External Cooperation Program of BIC, Chinese Academy of Sciences (No. 181231KYSB20130007). J. W. thanks the National 10000-Talent Program and the CAS 100-Talent Program for financial support. J. N. C. is supported by the ERC Grant SEMANTICS. W. J. B. is supported in part by Science Foundation Ireland (No. 12/IA/1306).

REFERENCES

1. G. Cunningham, M. Lotya, C. S. Cucinotta, S. Sanvito, S. D. Bergin, R. Menzel, M. S. Shaffer, and J. N. Coleman, "Solvent exfoliation of transition metal dichalcogenides: dispersibility of exfoliated nanosheets varies only weakly between compounds," ACS Nano **6**, 3468–3480 (2012).
2. R. Gordon, D. Yang, E. Crozier, D. Jiang, and R. Frindt, "Structures of exfoliated single layers of WS_2, MoS_2, and $MoSe_2$ in aqueous suspension," Phys. Rev. B **65**, 125407 (2002).
3. S. Tongay, J. Zhou, C. Ataca, J. Liu, J. S. Kang, T. S. Matthews, L. You, J. Li, J. C. Grossman, and J. Wu, "Broad-range modulation of light emission in two-dimensional semiconductors by molecular physisorption gating," Nano Lett. **13**, 2831–2836 (2013).
4. N. Peimyoo, J. Shang, C. Cong, X. Shen, X. Wu, E. K. Yeow, and T. Yu, "Nonblinking, intense two-dimensional light emitter: monolayer WS_2 triangles," ACS Nano **7**, 10985–10994 (2013).
5. P. Tonndorf, R. Schmidt, P. Böttger, X. Zhang, J. Börner, A. Liebig, M. Albrecht, C. Kloc, O. Gordan, and D. R. Zahn, "Photoluminescence emission and Raman response of monolayer MoS_2, $MoSe_2$, and WSe_2," Opt. Express **21**, 4908–4916 (2013).
6. M. Bernardi, M. Palummo, and J. C. Grossman, "Extraordinary sunlight absorption and one nanometer thick photovoltaics using two-dimensional monolayer materials," Nano Lett. **13**, 3664–3670 (2013).
7. L. M. Malard, T. V. Alencar, A. P. M. Barboza, K. F. Mak, and A. M. de Paula, "Observation of intense second harmonic generation from MoS_2 atomic crystals," Phys. Rev. B **87**, 201401 (2013).
8. K. Wang, J. Wang, J. Fan, M. Lotya, A. O'Neill, D. Fox, Y. Feng, X. Zhang, B. Jiang, and Q. Zhao, "Ultrafast saturable absorption of two-dimensional MoS_2 nanosheets," ACS Nano **7**, 9260–9267 (2013).
9. R. Wu, Y. L. Zhang, S. C. Yan, F. Bian, W. L. Wang, X. D. Bai, X. H. Lu, J. M. Zhao, and E. G. Wang, "Purely coherent nonlinear optical response in solution dispersions of graphene sheets," Nano Lett. **11**, 5159–5164 (2011).
10. W. Ji, W. Chen, S. Lim, J. Lin, and Z. Guo, "Gravitation-dependent, thermally-induced self-diffraction in carbon nanotube solutions," Opt. Express **14**, 8958–8966 (2006).
11. T. Sekine, T. Nakashizu, K. Toyoda, K. Uchinokura, and E. Matsuura, "Raman scattering in layered compound 2H-WS_2," Solid State Commun. **35**, 371–373 (1980).
12. S. Sugai, T. Ueda, and K. Murase, "Raman-scattering in Mos_2, $MoSe_2$ and alpha-$Mote_2$ at high-pressures," J. Phys. Colloq. **42**, 320–322 (1981).
13. N. McDevitt, J. Zabinski, and M. Donley, "The use of Raman scattering to study disorder in pulsed laser deposited MoS_2 films," Thin Solid Films **240**, 76–81 (1994).
14. S.-L. Li, H. Miyazaki, H. Song, H. Kuramochi, S. Nakaharai, and K. Tsukagoshi, "Quantitative Raman spectrum and reliable thickness identification for atomic layers on insulating substrates," ACS Nano **6**, 7381–7388 (2012).
15. H. R. Gutierrez, N. Perea-Lopez, A. L. Elias, A. Berkdemir, B. Wang, R. Lv, F. Lopez-Urias, V. H. Crespi, H. Terrones, and M. Terrones, "Extraordinary room-temperature photoluminescence in triangular WS_2 monolayers," Nano Lett. **13**, 3447–3454 (2013).
16. A. Berkdemir, H. R. Gutiérrez, A. R. Botello-Méndez, N. Perea-López, A. L. Elías, C. Chia, B. Wang, V. H. Crespi, F. López-Urías, and J. Charlier, "Identification of individual and few layers of WS_2 using Raman spectroscopy," Sci. Rep. **3**, 1755 (2013).
17. S. D. Durbin, S. M. Arakelian, and Y. R. Shen, "Laser-induced diffraction rings from a nematic-liquid-crystal film," Opt. Lett. **6**, 411–413 (1981).
18. G. Wang, S. Zhang, F. A. Umran, X. Cheng, N. Dong, D. Coghlan, Y. Cheng, L. Zhang, W. J. Blau, and J. Wang, "Tunable effective nonlinear refractive index of graphene dispersions during the distortion of spatial self-phase modulation," Appl. Phys. Lett. **104**, 141909 (2014).
19. Z. Wang, "Alignment of graphene nanoribbons by an electric field," Carbon **47**, 3050–3053 (2009).
20. R. Karimzadeh, "Spatial self-phase modulation of a laser beam propagating through liquids with self-induced natural convection flow," J. Opt. **14**, 095701 (2012).
21. C. M. Vest and M. L. Lawson, "Onset of convection near a suddenly heated horizontal wire," Int. J. Heat Mass Transfer **15**, 1281–1283 (1972).
22. S. Wang, H. Yu, H. Zhang, A. Wang, M. Zhao, Y. Chen, L. Mei, and J. Wang, "Broadband few-layer MoS_2 saturable absorbers," Adv. Mater. **26**, 3538–3544 (2014).
23. N. Kumar, Q. Cui, F. Ceballos, D. He, Y. Wang, and H. Zhao, "Exciton-exciton annihilation in $MoSe_2$ monolayers," Phys. Rev. B **89**, 125427 (2014).
24. W. Li, J. Carrete, and N. Mingo, "Thermal conductivity and phonon linewidths of monolayer MoS_2 from first principles," Appl. Phys. Lett. **103**, 253103 (2013).
25. F. Wurthner, S. Yao, J. Schilling, R. Wortmann, M. Redi-Abshiro, E. Mecher, F. Gallego-Gomez, and K. Meerholz, "ATOP dyes. Optimization of a multifunctional merocyanine chromophore for high refractive index modulation in photorefractive materials," J. Am. Chem. Soc. **123**, 2810–2824 (2001).
26. B. R. Bennett, R. A. Soref, and J. A. Delalamo, "Carrier-induced change in refractive-index of InP, GaAs, and InGaAsP," IEEE J. Quantum Electron. **26**, 113–122 (1990).